Energy Advances

Accepted Manuscript

This article can be cited before page numbers have been issued, to do this please use: D. Aloysius, M. Khan, A. Mondal and S. Gupta, *Energy Adv.*, 2024, DOI: 10.1039/D4YA00338A.

ROYAL SOCIETY OF CHEMISTRY

rsc.li/energy-advances

Effect of PCBM nanoparticles in Lead-based Layered $(PEA)_2PbI_4$ Perovskite Thin Films

Deepak Aloysius,[†] Muskan Khan,[†] Arindam Mondal,[†] Satyajit Gupta*[†]

[†] Department of Chemistry, Indian Institute of Technology Bhilai, Durg, Chhattisgarh, 491002

*Corresponding Author

Email: satyajit@iitbhilai.ac.in

Abstract

Two-dimensional (2D) layered halide perovskites are considered to be one of the future potential semiconductor materials due to their higher moisture stability than three-dimensional (3D) perovskites. However, improving this material's optical and electrical properties is still necessary for critical applications. The technique of additive engineering can be utilized to tune and enhance the optoelectrical properties of the 2D perovskites. This work studies the impact of mixing a certain amount of a fullerene derivative '[6,6]-Phenyl C_{61}-Butyric acid Methyl ester' (PCBM) into 2D $(PEA)_2PbI_4$ perovskite thin films (PEA=Phenyl Ethyl Ammonium). The studies show that PCBM does not affect the structure and bandgap of the $(PEA)_2PbI_4$ perovskite. On the other hand, PCBM improves photoluminescence emission intensity and promotes charge separation at the perovskite/PCBM interface. Further studies convey that, even though PCBM can heal certain defect states in the $(PEA)_2PbI_4$ perovskite material, the electrons generated over-illumination at the perovskite/PCBM interface are trapped by this fullerene derivative. Hence, PCBM plays a dual role when mixed with $(PEA)_2PbI_4$ perovskite, as (1) a defect healing agent, and (2) an electron acceptor. Although, over continuous illumination on the $(PEA)_2PbI_4$ perovskite thin films, the photoexcited electrons are trapped by PCBM. As a result, the photocurrent response and the photocatalytic rate get reduced in PCBM mixed $(PEA)_2PbI_4$ perovskite thin films.

Keywords: Fullerene, Semiconductor, Layered Perovskites, Thin film, Photoelectrochemistry

View Article Online
DOI: 10.1039/D4YA00338A

Introduction

The successive developments in $APbX_3$ type [A=inorganic monocations such as Caesium ion (Cs^+) and organic monocations such as Methyl ammonium ($CH_3NH_3^+$), etc., X= halides such as iodide (I^-), bromide (Br^-), mixed halide or pseudohalides such as thiocyanate (SCN^-), etc.[1–6]] perovskite semiconductors made them one of the promising candidates among third-generation solar cell devices.[7] Further, the reporting of Cao *et al.* on two-dimensional (2D) halide perovskites opened the path toward another class of perovskite semiconductors.[8] Along with the existing properties of 3D perovskites, such as high absorption coefficient,[9] intense photoluminescence[10] etc., the main advantage of 2D perovskites is their relatively higher moisture stability.[11] The large hydrophobic organic cations in 2D perovskites act as a barrier for moisture intervention.[12] However, the wide optical bandgap[13] and low charge transport[14] are the major drawbacks of 2D perovskites. The technique of additive engineering has been utilized in 3D perovskites to better its optoelectronic properties.[15–20] In 2D perovskites, optoelectrical properties can be fine-tuned using the same additive engineering technique.[21] Earlier, *Zhang et al.* reported that Cs^+ doping in $(BA)_2(MA)_3Pb_4I_{13}$ perovskite solar cells boost the power conversion efficiency (PCE) by more than 1% with better humidity resistance.[22] Further, *Zhang et al.* reported that after MACl doping, the $BA_2MA_4Pb_5I_{16}$ layered perovskite films showed improved PCE and operational stability.[23] This work studies the effect of mixing a fullerene derivative '[6,6]-phenyl C_{61}-butyric acid methyl ester' (PCBM) nanoparticles into a 2D perovskite.

Several research groups have already established using PCBM nanoparticles in organic solar cells to facilitate exciton separation.[24–26] The high solubility and the electron-accepting nature are the significant properties that promote the use of PCBM in photovoltaic materials.[27] After the establishment of perovskite photovoltaics, the PCBM is used as an Electron Transport Layer (ETL) in perovskite solar cell devices. *You et al.* reported the fabrication of $CH_3NH_3PbI_{3-x}Cl_x$ based flexible solar cell devices using PCBM as ETL and achieved a PCE of 9.2%.[28] *Heo et al.* reported the fabrication of $MAPbI_3$ based perovskite solar cells with PCBM as ETL, which has an average PCE of 18.1%.[29] Similarly, several reports have been made of using the PCBM ETL in low-temperature processed perovskite solar cell

View Article Online
DOI: 10.1039/D4YA00338A

devices with p-i-n architecture.[30–34] Further, some reports show the effect on 2D perovskite films by the PCBM layer interface. *Yang et al.* reported that at $(PEA)_2(MA)_{n-1}Pb_nI_{3n+1}$/PCBM interface, the phenethylammonium iodide (PEAI) ligand promotes better transfer of electrons from perovskite crystal to the PCBM layer.[35] *Shen et al.* reported the efficient and fast charge transfer dynamics in 2D $CsPbBr_3$ nanosheets and PCBM layer heterojunctions.[36] *Wei et al.* reported efficient charge separation at multiple quantum well (MQW) perovskite/PCBM interface.[37]

This work reports the effect of mixing varying amounts of PCBM nanoparticles in $(PEA)_2PbI_4$ perovskite [where phenylethylammonium ion (PEA^+) is the organic cation], which has not been reported before to the best of our knowledge. Even though $(PEA)_2PbI_4$ perovskites have firmly bound excitons[38], it is observed that PCBM helps the separation of excitons at the PCBM/perovskite interface in the mixed form. Further, we found that PCBM cannot influence the structure and bandgap of the $(PEA)_2PbI_4$ perovskite. On the other hand, PCBM improves the photoluminescence emission intensity and reduces the charge carrier lifetime.

View Article Online
DOI: 10.1039/D4YA00338A

Experimental section

Materials

Lead iodide (99%), 2-Phenylethylamine solution (≥99%), Hydriodic acid (57 wt. % in H_2O, distilled, stabilized, 99.95%) Dimethyl sulfoxide (ACS reagent, ≥ 99.9%), N,N-Dimethyl formamide (ACS reagent, ≥99.8%), Toluene (99.8%), PCBM (>99.5%), Tetrabutylammonium hexafluorophosphate [$(Bu_4N)^+(PF_6)^-$] (≥98%), Dichloromethane (anhydrous, ≥99.8%) 2-Mercaptobenzothiazole (97%), Hexane (anhydrous, 95%), Hypophosphorous acid solution (50 wt% in H_2O), Titanium isopropoxide (97%), Diethanolamine (reagent grade, ≥98%), Diethyl ether (≥99.9%) were purchased from Sigma-Aldrich. Triphenylphosphine oxide (>98%) was purchased from Spectrochem, and silica was purchased from Loba Chemie. Acetone (99.9%) was purchased from Rankem. Ethanol (99.9%) and plain glass slides were purchased from a local supplier. FTO (Fluorine-doped Tin Oxide) coated glass slides were purchased from Feeniks Technologies (transparency >85%). All the chemicals are used without further purification.

Material Characterization

The perovskite thin films were fabricated using the EZspin-A1 Apex Spin Coater. The grazing incidence X-ray Diffraction (GIXRD) analysis was done with the Bruker D8 Advance X-ray diffractometer using Cu 'Kα' radiation of wavelength 1.54 Å at 40 mA current & 40 kV potential. The UV-visible spectroscopic analysis was conducted using Shimadzu UV-2600. Further, the Steady State Photo-Luminescence (SSPL) analysis was carried out using Fluorolog FL3-211 HORIBA Scientific with a 450-watt Xenon arc lamp. Time-resolved photoluminescence (TRPL) analysis was carried out using the HORIBA Scientific DeltaFlex™ and DeltaPro™ Fluorescence Lifetime Systems using the 453 nm laser excitation pulse (EZTime software was used for TRPL analysis). The Field Emission Scanning Electron Microscope (FESEM) images of the perovskite thin films were captured using Zeiss Gemini SEM500 instruments. The High-Resolution Transmission Electron Microscopy (HRTEM) images were captured using JEOL & JEM-F200 (CF-HR). The photoelectrochemistry-related experiments are carried out using Metrohm Dropsens μStat-i 400s potentiostat (with the Dropview 8400 software). The perovskite thin film was illuminated using a calibrated solar simulator (Model, ScienceTech) with a light intensity equivalent to one sun (1.5 AM). Also,

View Article Online
DOI: 10.1039/D4YA00338A

the photocatalytic experiments were conducted using a white Light Emitting Diode (LED) source. All analyses are performed over perovskite thin film fabricated over glass substrates, except for the photoelectrochemical analyses where the FTO substrate was used.

Synthesis of Phenylethylammonium iodide (PEAI)

The equimolar concentration of Phenylethyl amine solution and Hydriodic acid (HI) was neutralized in 10 ml ethanol medium at low temperature (ice bath). 1 ml of Hypophosphorous acid solution (H_3PO_2) was added to prevent the oxidation of iodide ions. The reaction was kept for 4 hours, and a white powder of PEAI was obtained after evaporating the solvent (ethanol), washing (with diethyl ether), filtering, and drying.

Synthesis of PCBM mixed $(PEA)_2PbI_4$ perovskite precursor solution

A 2:1 molar ratio of PEAI and Lead iodide (PbI_2) was dissolved in the mixture of N, N Dimethyl formamide (DMF), and Dimethyl sulfoxide (DMSO) solvents in the ratio 8:2 under constant stirring for 4 hours at 60ºC. An orange solution was obtained. A thoroughly dispersed PCBM solution (in the same solvent ratio as the precursor solution) was added to the perovskite precursor solution as per the composition and further sonicated for 1 hour. The PCBM nanoparticles occupy as spherical aggregates when dispersed in the solvent mixture (Fig. S1).

Fabrication of PCBM mixed $(PEA)_2PbI_4$ perovskite thin films:

Both glass slides (2.5 cm x 2 cm) and FTO films (2 cm x 2 cm) are used as substrates for thin film fabrication. The substrate was cleaned with soap and sonicated in distilled water, acetone, and ethanol for 10 minutes each. Further, the substrates are dried under a hot air gun. These cleaned substrates are preheated at 90ºC for 5 minutes. Then, the substrate was loaded in a spin coater, and 200 µL of precursor solution was spread over the glass substrate (150 µL precursor solution was used for the FTO substrate). After that, the perovskite thin films were fabricated via spin coating at 4000 rpm for 20 seconds. The antisolvent toluene was added at the 15th second. The perovskite thin films were heated at 100°C for 10 minutes in the last step.

View Article Online
DOI: 10.1039/D4YA00338A

Synthesis and fabrication of compact Titania layer (c-TiO_2)

An equimolar mixture (0.5 M) of Titanium isopropoxide [$Ti(OCH(CH_3)_2)_4$] and Diethanolamine [$NH(CH_2CH_2OH)_2$] was dissolved in ethanol (5 ml) by rigorous stirring for 15 minutes. The solution turns from white to colorless. The resulting solution was spin-coated over the FTO substrate at 7000 rpm for 30 seconds, then annealed at 500°C for 2 hours.

View Article Online
DOI: 10.1039/D4YA00338A

Result and Discussion

Structure and Bandgap

The PCBM nanoparticles mixed $(PEA)_2PbI_4$ perovskite thin films are fabricated via a one-step spin coating technique. A uniform thin film was obtained for all the compositions over the substrate (Fig. S2). In this work, the thin films fabricated using the following precursor solutions are analyzed: P_0= pristine $(PEA)_2PbI_4$, $P_{0.5}$ = 0.5 mg PCBM mixed in 1 ml $(PEA)_2PbI_4$ perovskite precursor, and $P_{0.75}$= 0.75 mg PCBM mixed in 1 ml $(PEA)_2PbI_4$ perovskite precursor solution.

The GIXRD of all compositions (P_0, $P_{0.5}$, and $P_{0.75}$) was carried out to determine the polycrystalline structure. The diffraction data shows periodic peaks along *(00l)* planes (Fig. 1a), which signifies the layered orientation of PbI_4^{2-} moieties in $(PEA)_2PbI_4$ perovskite thin films (Fig. 1b).[39] Also, no peak shift is observed in all the compositions, which indicates that PCBM does not affect the $(PEA)_2PbI_4$ perovskite structure.

Further, all compositions of $(PEA)_2PbI_4$ perovskite thin films show significant absorption in the visible region of the spectrum (Fig. S3). Also, an increase in absorbance is observed for $P_{0.5}$ and $P_{0.75}$ compositions. This observation indicates that the black PCBM is evenly dispersed over the $(PEA)_2PbI_4$ perovskite thin films. Further, the bandgap of all compositions (P_0, $P_{0.5}$, and $P_{0.75}$) was calculated from the Tauc plot using the Kubalka-Munk function $[(\alpha h\upsilon)^2$ vs. $h\upsilon$, where 'α' is the absorption coefficient] using transmittance data (Fig. 1c). It was observed that the bandgap remains at 2.36 eV for all compositions (Fig. S4a-c). Therefore, the PCBM mixing does not create structural distortion in $(PEA)_2PbI_4$ perovskite thin films.

View Article Online
DOI: 10.1039/D4YA00338A

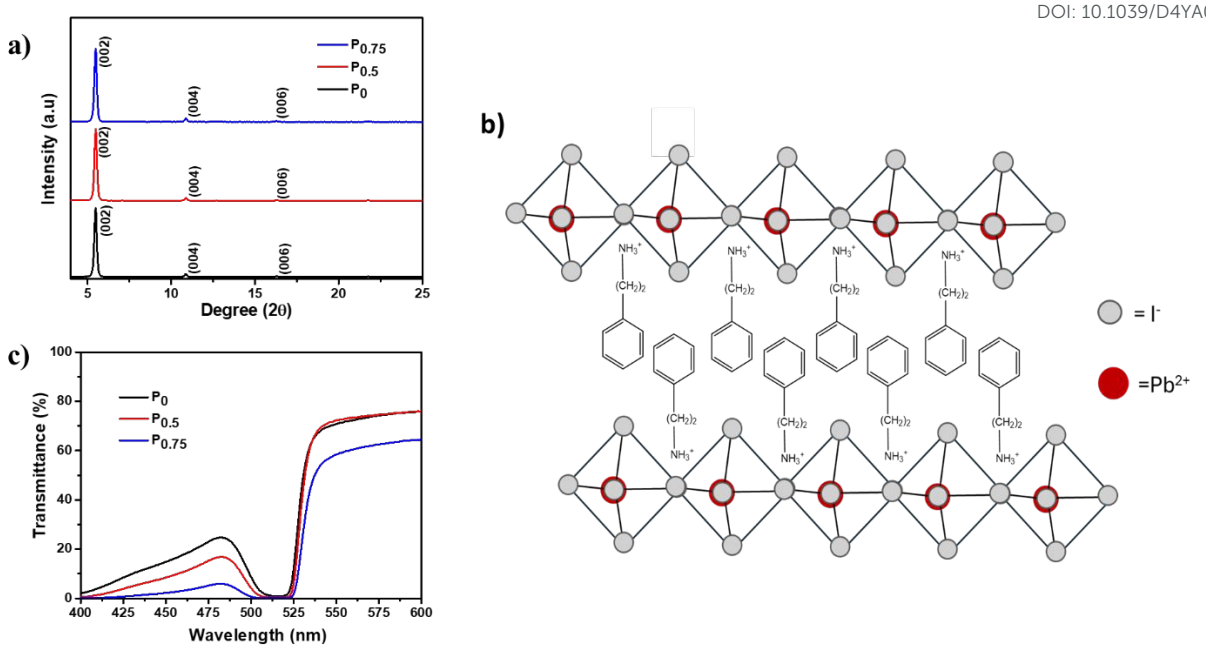

Fig. 1: a) XRD analysis of P_0, $P_{0.5}$, and $P_{0.75}$ perovskite thin films. b) Layered structure of $(PEA)_2PbI_4$ perovskite c) Transmittance analyses of P_0, $P_{0.5}$, and $P_{0.75}$ compositions. [P_0= pristine $(PEA)_2PbI_4$, $P_{0.5}$ = 0.5 mg PCBM mixed in 1 ml $(PEA)_2PbI_4$ perovskite precursor, and $P_{0.75}$= 0.75 mg PCBM mixed in 1 ml $(PEA)_2PbI_4$ perovskite precursor solution.]

Morphological and Optical properties

The surface morphology and thickness of the PCBM nanoparticle mixed $(PEA)_2PbI_4$ perovskite thin films were analyzed using SEM images (Fig. 2a-c). This analysis shows that the perovskite films are packed and pinhole-free. Also, the thickness of the films is within a range of 450 nm to 500 nm. On analyzing the film morphology, P_0 composition generates more uniform films, and roughness increases at the surface of the PCBM nanoparticle mixed $(PEA)_2PbI_4$ perovskite thin films ($P_{0.5}$ and $P_{0.75}$).

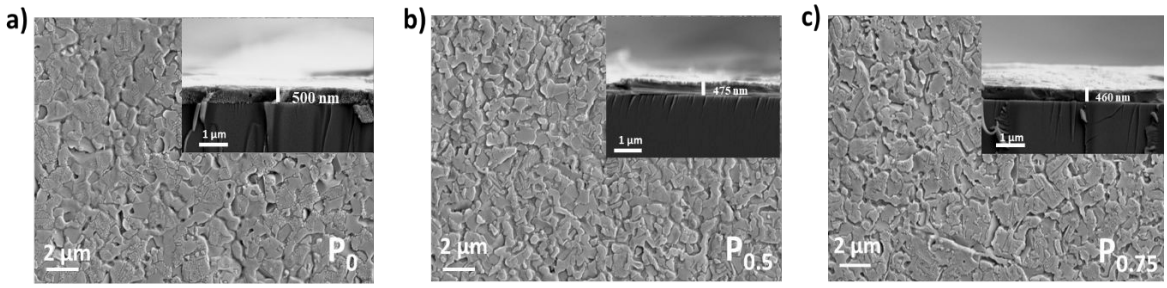

Fig. 2: Surface and cross-sectional images (given in the inset) of a)P_0, b) $P_{0.5}$, c) $P_{0.75}$ compositions. [P_0= pristine $(PEA)_2PbI_4$, $P_{0.5}$ = 0.5 mg PCBM mixed in 1 ml $(PEA)_2PbI_4$

View Article Online
DOI: 10.1039/D4TA00338A

perovskite precursor, and $P_{0.75}$= 0.75 mg PCBM mixed in 1 ml $(PEA)_2PbI_4$ perovskite precursor solution.]

The Steady State Photo Luminescence (SSPL) analysis was carried out to understand charge carrier recombination intensity in the PCBM nanoparticles mixed $(PEA)_2PbI_4$ perovskite thin films (Fig. 3a). The emission peak of all the compositions (P_0, $P_{0.5}$, and $P_{0.75}$) is observed at the same wavelength of 529 nm, which agrees with the bandgap calculated from the Tauc plots (Fig. S4a-c). On the other hand, an increase in emission intensity is observed for $P_{0.5}$ and $P_{0.75}$ compositions. The higher PL intensity is attributed to the passivation of defect states over the PCBM nanoparticles mixed $(PEA)_2PbI_4$ perovskite films. Earlier, several reports show improvement in PL intensity due to defect passivation on different perovskite materials.[40,41] The $(PEA)_2PbI_4$ perovskites are reported to have undercoordinated Pb^{2+} ions in the surface and I^- defects in the bulk due to iodide migration.[42] Here, PCBM can passivate the defects by binding them at the grain boundaries and help in electron movement across the grains.[43] The $P_{0.5}$ composition has the highest PL intensity, which indicates that it is the optimum composition, showing the most defect passivation. A similar increase in PL intensity can also be observed when triphenylphosphine oxide (TOPO) is mixed in the $(PEA)_2PbI_4$ perovskite thin films (Fig. S5a). In TOPO, the lone pair electrons in the oxygen atom replace the iodide vacancies.[44] Conversely, the PL intensity remains unaffected with neutral materials such as silica particles mixed $(PEA)_2PbI_4$ perovskite films (Fig. S5b). These analyses indicate additive engineering techniques can influence the defect states in $(PEA)_2PbI_4$ perovskite thin films.

The Time-Resolved Photo Luminescence (TRPL) analysis was carried out to understand the charge recombination dynamics in the PCBM nanoparticles mixed $(PEA)_2PbI_4$ perovskite thin films (Fig. 3b). The average lifetime of the compositions is determined by fitting TRPL curves using the biexponential decay function [$y=A_1\exp(-t/\tau_1) + A_2\exp(-t/\tau_2)$]. Here, the average lifetime of P_0 (τ=246 ps) is higher than $P_{0.5}$ (τ=216 ps) and $P_{0.75}$ (τ=195 ps). The fitting data is given in Table S1. Here, PCBM plays the role of an electron acceptor by collecting the excited electrons from $(PEA)_2PbI_4$ perovskite, thereby reducing the charge recombination lifetime. Upon analysis of the SSPL and TRPL data for PCBM nanoparticles mixed $(PEA)_2PbI_4$ perovskite compositions, the SSPL intensity increases for $P_{0.5}$ and $P_{0.75}$ compared to P_0. On the other hand, the TRPL lifetime decreases for $P_{0.5}$ and $P_{0.75}$ compared to P_0. This trend is due

to the dual behavior of PCBM in $(PEA)_2PbI_4$ perovskite: as a defect healing agent (from SSPL analysis) and as an electron acceptor (from TRPL analysis).

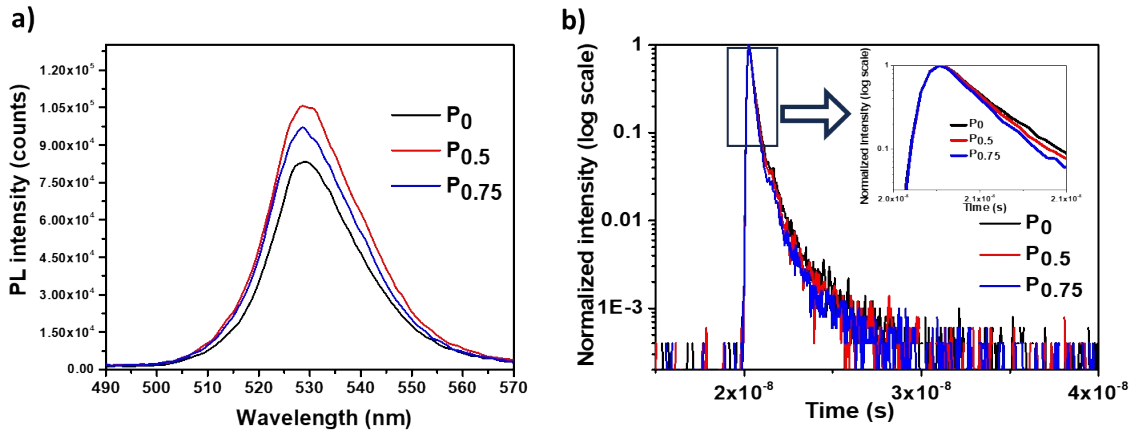

Fig. 3: a) SSPL and b) TRPL curves of P_0, $P_{0.5}$ and $P_{0.75}$ compositions.[P_0= pristine $(PEA)_2PbI_4$, $P_{0.5}$ = 0.5 mg PCBM mixed in 1 ml $(PEA)_2PbI_4$ perovskite precursor, and $P_{0.75}$= 0.75 mg PCBM mixed in 1 ml $(PEA)_2PbI_4$ perovskite precursor solution.]

Photoelectrochemical properties

The photoelectrochemical analysis was conducted to study the charge carrier dynamics of PCBM nanoparticle mixed $(PEA)_2PbI_4$ perovskite thin films within a multilayer system. The analysis was carried out using a three-electrode setup with 'Ag/AgCl' as the reference electrode, 'Pt' wire as the counter electrode, and the multilayered perovskite thin film as the working electrode (Fig. S6). Along with that, 0.1 M $[(Bu_4N)^+(PF_6)^-]$ dissolved in Dichloromethane (DCM) solvent was used as the supporting electrolyte, and a calibrated solar stimulator of 1 sun intensity functioned as the light source. The thin films are fabricated as glass/FTO/c-TiO_2/perovskite multilayers and illuminated from the glass side at a 10 cm distance from the solar simulator.

Initially, the chronoamperometric analysis was carried out for 3 minutes by chopping light at 0 V applied bias with respect to the Ag/AgCl reference electrode (Fig. 4a). The study shows a stable and significantly higher current is generated for P_0 (8.5 μA/cm^2) than for $P_{0.5}$ (3.8 μA/cm^2) and $P_{0.75}$ (1.6 μA/cm^2) compositions. A similar trend was observed for chronoamperometry analysis without the cTiO_2 layer (Fig. S7 a-c). Further, the Linear Sweep

View Article Online
DOI: 10.1039/D4YA00338A

Voltametric (LSV) analysis under illumination over a potential range of -0.2 V to 0.6 V shows a higher current response for P_0 composition (Fig. 4b). So, it is evident that the PCBM is trapping the photogenerated charge carriers from the $(PEA)_2PbI_4$ perovskite thin film and prevents its further movement within the system. Apart from that, the LSV curve signifies that the PCBM is improving the open circuit potential (V_{oc}) of the $(PEA)_2PbI_4$ perovskite thin film (Fig. 4b inset). The improved V_{oc} is attributed to the defect passivation effect of PCBM, as observed from SSPL analysis (discussed earlier in Fig. 3a). Earlier reports on different perovskite materials suggest the improvement of V_{oc} through defect healing.[45]

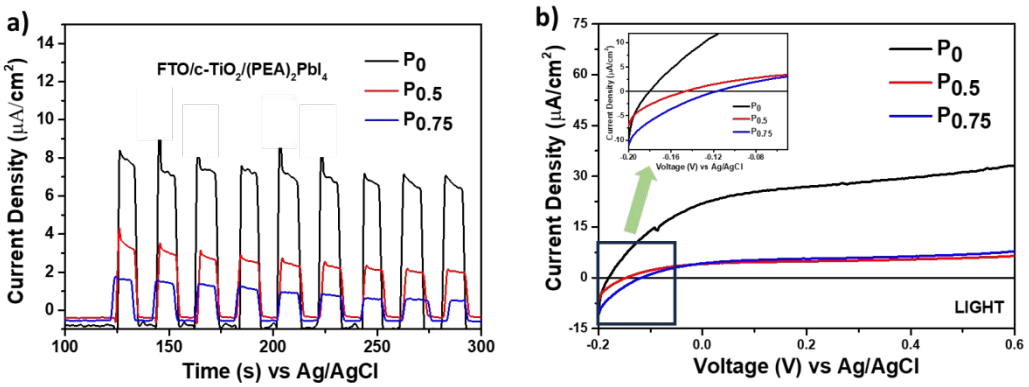

Fig. 4: a) The chronoamperometric and b) LSV curves (over c-TiO_2) of P_0, $P_{0.5}$, and $P_{0.75}$ compositions.[P_0= pristine $(PEA)_2PbI_4$, $P_{0.5}$ = 0.5 mg PCBM mixed in 1 ml $(PEA)_2PbI_4$ perovskite precursor, and $P_{0.75}$= 0.75 mg PCBM mixed in 1 ml $(PEA)_2PbI_4$ perovskite precursor solution.]

Photocatalytic properties

The photocatalytic activity of PCBM nanoparticles mixed $(PEA)_2PbI_4$ perovskite thin films was studied on 2-mercaptobenzothiazole (MBT) dye to understand the behavior of excitons within the material. The photocatalytic experiment was carried out with perovskite thin films coated over a glass slide. A strip of a perovskite thin film-coated glass slide (2 cm x 0.5cm) was dipped in the MBT dye-filled quartz cuvette and illuminated with white LED. Further, the absorbance of MBT dye was analyzed every 15 minutes for three cycles.

The MBT dye undergoes an oxidative S-S coupling reaction under illumination in the presence of a photocatalyst, forming 2,2'-Dithiobis(benzothiazole) (MBTS).[46,47] The holes generated from the $(PEA)_2PbI_4$ perovskite excitation catalyze the coupling reaction.[48] The photocatalysis

reaction rate of each composition is directly correlated with the reduction absorption peak intensity at each 15-minute interval (Fig. S8). Further, the rate constant (k) was determined from the slope of $\boldsymbol{In\frac{At}{A0}\ vs\ t}$ plot where A denotes the absorbance and t denotes the irradiation time (Fig. 5). The absorbance analysis shows that the photocatalytic S-S coupling reaction rate is higher for the P_0 (0.055 min^{-1}) composition than the $P_{0.5}$ (0.04 min^{-1}) and $P_{0.75}$ (0.041 min^{-1}) compositions. The formation of MBTS was confirmed using the Electrospray ionization mass spectroscopy (ESI-MS) analysis of the dye. (Fig. S9). This observation indicates that relatively fewer holes are available for catalyzing the coupling reaction in PCBM nanoparticle mixed $(PEA)_2PbI_4$ perovskite thin film compositions ($P_{0.5}$ and $P_{0.75}$). Here, PCBM traps the photoexcited electrons of $(PEA)_2PbI_4$ perovskite and promotes faster recombination with holes. This process eventually reduces the reaction rate due to the decline in excitons of $(PEA)_2PbI_4$ perovskite photocatalyst. Also, the higher roughness of $P_{0.5}$ and $P_{0.75}$ thin film compositions can reduce the photocatalysis reaction rate. (as observed in Fig. 2)

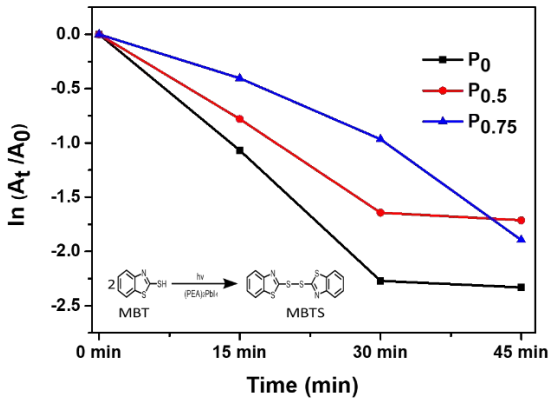

Fig. 5: Photocatalytic coupling reaction rate of MBT dye in P_0, $P_{0.5}$, and $P_{0.75}$ compositions at 15-minute intervals (the MBT coupling reaction is given in the inset).[P_0= pristine $(PEA)_2PbI_4$, $P_{0.5}$ = 0.5 mg PCBM mixed in 1 ml $(PEA)_2PbI_4$ perovskite precursor, and $P_{0.75}$= 0.75 mg PCBM mixed in 1 ml $(PEA)_2PbI_4$ perovskite precursor solution.]

View Article Online
DOI: 10.1039/D4YA00338A

Conclusion

This work delineates the effect of PCBM nanoparticle mixing in $(PEA)_2PbI_4$ perovskite thin films with three different compositions (P_0, $P_{0.5}$, and $P_{0.75}$). All the compositions form a layered structure with the same bandgap. However, roughness increases for PCBM mixed $(PEA)_2PbI_4$ perovskite thin film compositions ($P_{0.5}$ and $P_{0.75}$). Also, the SSPL emission intensity increases considerably for $P_{0.5}$ and $P_{0.75}$ compositions, which indicates that PCBM helps passivate the defect states at the grain boundaries. On the other hand, the TRPL analysis indicates that recombination lifetime declined for $P_{0.5}$ and $P_{0.75}$ compositions, which is attributed to PCBM's electron-accepting behavior. The discrepancy in the increase in SSPL intensity and the decrease in TRPL lifetime signifies the two independent behaviors of PCBM nanoparticles impacting $(PEA)_2PbI_4$ perovskite thin film properties transiently. Further, the photoelectrochemistry analysis shows a significant reduction in the current generation in $P_{0.5}$ and $P_{0.75}$ compositions, even though there is an increase in V_{oc} due to defect passivation. Also, in the photocatalytic analysis, the reaction rate is lower for $P_{0.5}$ and $P_{0.75}$ compositions. All these observations signify that the PCBM is trapping the accepted electrons on continuous illumination on $(PEA)_2PbI_4$ perovskite thin films.

View Article Online
DOI: 10.1039/D4YA00338A

Associated Content

Supporting Information

The supporting information is available free of charge

Perovskite thin film images. UV absorbance data. TEM and SSPL analyses. TRPL fitting data. Additional details on photoelectrochemical experiments, and photocatalytic reaction with ESI-MS results.

Author Information

Corresponding Author

Satyajit Gupta – Assistant Professor, Department of Chemistry, Indian Institute of Bhilai, Chhattisgarh, India, Email: satyajit@iitbhilai.ac.in, orcid.org/ 0000-0002-5323-341X.

Authors

Deepak Aloysius – Department of Chemistry, Indian Institute of Bhilai, Chhattisgarh, India. Email: deepakaloysius@iitbhilai.ac.in, orcid.org/0009-0009-4532-4635

Muskan Khan - Department of Chemistry, Indian Institute of Bhilai, Chhattisgarh, India. Email: muskankhanj@iitbhilai.ac.in

Arindam Mondal – Department of Chemistry, Indian Institute of Bhilai, Chhattisgarh, India. Email: arindamm@iitbhilai.ac.in, orcid.org/0000-0001-5364-932X.

Notes

The authors declare no competing financial interest.

View Article Online
DOI: 10.1039/D4YA00338A

Acknowledgments

DA acknowledges the Ministry of Education, India (MoE) for the research fellowship. SG thanks SERB for the Start-up Research Grant (SRG/2019/000157).

References:

1 Y. Pan, Y. Zhang, W. Kang, N. Deng, Z. Yan, W. Sun, X. Kang and J. Ni, *Mater Adv*, 2022, **3**, 4053–4068.

2 M. A. Green, A. Ho-Baillie and H. J. Snaith, *Nat Photonics*, 2014, **8**, 506–514.

3 H.-S. Kim, C.-R. Lee, J.-H. Im, K.-B. Lee, T. Moehl, A. Marchioro, S.-J. Moon, R. Humphry-Baker, J.-H. Yum, J. E. Moser, M. Grätzel and N.-G. Park, *Sci Rep*, 2012, **2**, 591.

4 M. Kulbak, S. Gupta, N. Kedem, I. Levine, T. Bendikov, G. Hodes and D. Cahen, *J Phys Chem Lett*, 2016, **7**, 167–172.

5 D. P. McMeekin, G. Sadoughi, W. Rehman, G. E. Eperon, M. Saliba, M. T. Hörantner, A. Haghighirad, N. Sakai, L. Korte, B. Rech, M. B. Johnston, L. M. Herz and H. J. Snaith, *Science (1979)*, 2016, **351**, 151–155.

6 Q. Jiang, D. Rebollar, J. Gong, E. L. Piacentino, C. Zheng and T. Xu, *Angewandte Chemie International Edition*, 2015, **54**, 7617–7620.

7 J. Yan and B. R. Saunders, *RSC Adv.*, 2014, **4**, 43286–43314.

8 D. H. Cao, C. C. Stoumpos, O. K. Farha, J. T. Hupp and M. G. Kanatzidis, *J Am Chem Soc*, 2015, **137**, 7843–7850.

9 H. Wang, J. Ma and D. Li, *J Phys Chem Lett*, 2021, **12**, 8178–8187.

10 S. Chen and G. Shi, *Advanced Materials,* 2017, **29**, 1605448

11 I. C. Smith, E. T. Hoke, D. Solis-Ibarra, M. D. McGehee and H. I. Karunadasa, *Angewandte Chemie International Edition*, 2014, **53**, 11232–11235.

12 S. Yang, Y. Wang, P. Liu, Y.-B. Cheng, H. J. Zhao and H. G. Yang, *Nat Energy*, 2016, **1**, 15016.

13 E.-B. Kim, M. S. Akhtar, H.-S. Shin, S. Ameen and M. K. Nazeeruddin, *Journal of Photochemistry and Photobiology C: Photochemistry Reviews*, 2021, **48**, 100405.

14 F. Zhang, H. Lu, J. Tong, J. J. Berry, M. C. Beard and K. Zhu, *Energy Environ Sci*, 2020, **13**, 1154–1186.

15 A. Mahapatra, D. Prochowicz, M. M. Tavakoli, S. Trivedi, P. Kumar and P. Yadav, *J Mater Chem A Mater*, 2020, **8**, 27–54.

16 T. Li, Y. Pan, Z. Wang, Y. Xia, Y. Chen and W. Huang, *J Mater Chem A Mater*, 2017, **5**, 12602–12652.

17 F. Zhang and K. Zhu, *Adv Energy Mater*, 2020, **10**, 1902579.

18 Y. Wu, F. Xie, H. Chen, X. Yang, H. Su, M. Cai, Z. Zhou, T. Noda and L. Han, *Advanced Materials*, 2017, **29**, 1701073.

19 D. S. Mann, S. Thakur, S. S. Sangale, K.-U. Jeong, S.-N. Kwon and S.-J. Na, *Solar Energy Materials and Solar Cells*, 2024, **269**, 112768.

20 K. Nagasawa, T. Sano, V. N. Chau, K. Enomoto, Y. Okuyama, Y. Sayama, R. Oikawa, T. Chiba and J. Kido, *Adv Mater Interfaces*, 2024, **11**, 2300449

21 G. Grancini and M. K. Nazeeruddin, *Nat Rev Mater*, 2018, **4**, 4–22.

22 X. Zhang, X. Ren, B. Liu, R. Munir, X. Zhu, D. Yang, J. Li, Y. Liu, D.-M. Smilgies, R. Li, Z. Yang, T. Niu, X. Wang, A. Amassian, K. Zhao and S. (Frank) Liu, *Energy Environ Sci*, 2017, **10**, 2095–2102.

23 F. Zheng, C. Zuo, M. Niu, C. Zhou, S. J. Bradley, C. R. Hall, W. Xu, X. Wen, X. Hao, M. Gao, T. A. Smith and K. P. Ghiggino, *ACS Appl Mater Interfaces*, 2020, **12**, 25980–25990.

24 F. Padinger, R. S. Rittberger and N. S. Sariciftci, *Adv Funct Mater*, 2003, **13**, 85–88.

25 T. Erb, U. Zhokhavets, G. Gobsch, S. Raleva, B. Stühn, P. Schilinsky, C. Waldauf and C. J. Brabec, *Adv Funct Mater*, 2005, **15**, 1193–1196.

26 Y. Kim, S. A. Choulis, J. Nelson, D. D. C. Bradley, S. Cook and J. R. Durrant, *Appl Phys Lett*, 2005, **86**, 063502.

27 C. J. Brabec, A. Cravino, D. Meissner, N. S. Sariciftci, T. Fromherz, M. T. Rispens, L. Sanchez and J. C. Hummelen, *Adv Funct Mater*, 2001, **11**, 374–380.

28 J. You, Z. Hong, Y. (Michael) Yang, Q. Chen, M. Cai, T.-B. Song, C.-C. Chen, S. Lu, Y. Liu, H. Zhou and Y. Yang, *ACS Nano*, 2014, **8**, 1674–1680.

29 J. H. Heo, H. J. Han, D. Kim, T. K. Ahn and S. H. Im, *Energy Environ Sci*, 2015, **8**, 1602–1608.

30 Z. Liu, L. Krückemeier, B. Krogmeier, B. Klingebiel, J. A. Márquez, S. Levcenko, S. Öz, S. Mathur, U. Rau, T. Unold and T. Kirchartz, *ACS Energy Lett*, 2019, **4**, 110–117.

31 W. Chen, Y. Wu, J. Liu, C. Qin, X. Yang, A. Islam, Y.-B. Cheng and L. Han, *Energy Environ Sci*, 2015, **8**, 629–640.

32 C. Tao, S. Neutzner, L. Colella, S. Marras, A. R. Srimath Kandada, M. Gandini, M. De Bastiani, G. Pace, L. Manna, M. Caironi, C. Bertarelli and A. Petrozza, *Energy Environ Sci*, 2015, **8**, 2365–2370.

33 F. Fu, T. Feurer, T. Jäger, E. Avancini, B. Bissig, S. Yoon, S. Buecheler and A. N. Tiwari, *Nat Commun*, 2015, **6**, 8932.

34 C.-H. Chiang and C.-G. Wu, *Nat Photonics*, 2016, **10**, 196–200.

35 J. Yang, S. Xiong, J. Song, H. Wu, Y. Zeng, L. Lu, K. Shen, T. Hao, Z. Ma, F. Liu, C. Duan, M. Fahlman and Q. Bao, *Adv Energy Mater*, 2020, **10**, 2000687.

36 Y. Shen, D. Yu, X. Wang, C. Huo, Y. Wu, Z. Zhu and H. Zeng, *Nanotechnology*, 2018, **29**, 085201.

37 Y. Wei, M. Li, R. Li, L. Zhang, R. Yang, W. Zou, Y. Cao, M. Xu, C. Yi, N. Wang, J. Wang and W. Huang, *Appl Phys Lett*, 2018, **113**, 041103.

38 H. Fang, J. Yang, S. Adjokatse, E. Tekelenburg, M. E. Kamminga, H. Duim, J. Ye, G. R. Blake, J. Even and M. A. Loi, *Adv Funct Mater*, 2020, **30**, 1907979.

39 D. B. Mitzi, *J Mater Chem*, 2004, **14**, 2355.

40 Yukta, M. K. Chini, R. Ranjan and S. Satapathi, *ACS Appl Electron Mater*, 2021, 3, 1572–1582.

41 S. A. Fateev, D. E. Belikova, P. A. Ivlev, N. A. Belich, K. A. Lyssenko, E. G. Maksimov, E. A. Goodilin and A. B. Tarasov, *Chemistry of Materials*, 2022, 34, 2998–3005.

42 J. Yin, R. Naphade, L. Gutiérrez Arzaluz, J.-L. Brédas, O. M. Bakr and O. F. Mohammed, *ACS Energy Lett*, 2020, **5**, 2149–2155.

43 J. Xu, A. Buin, A. H. Ip, W. Li, O. Voznyy, R. Comin, M. Yuan, S. Jeon, Z. Ning, J. J. McDowell, P. Kanjanaboos, J.-P. Sun, X. Lan, L. N. Quan, D. H. Kim, I. G. Hill, P. Maksymovych and E. H. Sargent, *Nat Commun*, 2015, **6**, 7081.

44 W. Li, X. Lai, F. Meng, G. Li, K. Wang, A. K. K. Kyaw and X. W. Sun, *Solar Energy Materials and Solar Cells*, 2020, **211**, 110527.

45 S. Wu, J. Zhang, Z. Li, D. Liu, M. Qin, S. H. Cheung, X. Lu, D. Lei, S. K. So, Z. Zhu and Alex. K.-Y. Jen, *Joule*, 2020, **4**, 1248–1262.

46 D. Cardenas-Morcoso, A. F. Gualdrón-Reyes, A. B. Ferreira Vitoreti, M. García-Tecedor, S. J. Yoon, M. Solis de la Fuente, I. Mora-Seró and S. Gimenez, *J Phys Chem Lett*, 2019, **10**, 630–636.

47 W.-B. Wu, Y.-C. Wong, Z.-K. Tan and J. Wu, *Catal Sci Technol*, 2018, **8**, 4257–4263.

48 A. Mondal, A. Lata, A. Prabhakaran and S. Gupta, *Mater Adv*, 2021, **2**, 5712–5722.

- The data supporting this article have been included as part of the Supplementary Information.

View Article Online
DOI: 10.1039/D4YA00338A